CFD investigation on thermal-hydraulic characteristics of a helical cruciform fuel bundle

Hangbin Zhao [a,b,c,*], Qi Zhang [c], Hanyang Gu [c], Yao Xiao [c], Maolong Liu [c]

[a] College of Astronautics, Nanjing University of Aeronautics and Astronautics, Nanjing, 211106, China
[b] Key Laboratory of Nuclear Technology Application and Radiation Protection in Astronautics, Ministry of Industry and Information Technology, Nanjing, 211106, China
[c] School of Nuclear Science and Engineering, Shanghai Jiao Tong University, Shanghai, 200240, China

ARTICLE INFO

ABSTRACT

The thermal-hydraulic performance of nuclear fuel has a very important effect on the safety and economy of a reactor. The helical cruciform fuel (HCF) is an innovative fuel design with a lot of potential advantages. HCF assembly is a self-supporting assembly. It needn't spacer grid which is usually used in the cylindrical fuel assembly. It has larger surface-to-volume ratio in comparison to the cylindrical fuel, which can increase the power output without necessarily altering the operating surface heat flux. In this research, the thermal-hydraulic characteristics of a 4 × 4 HCF bundle were investigated by numerical method. A numerical model of the bundle was developed and validated with experimental data. Based on this model, five flow conditions were respectively calculated. The transverse flow in the HCF bundle was analyzed, and the temperature distributions of the bundle and the water were discussed. The results show that the transverse mixing of water in the bundle is enhanced due to the helical geometry of the HCF rod. The mixing intensity periodically varies with twist angle increasing, and every twist angle of 90° is a variation cycle. The temperature distribution on the rod surface helically varies along the flow direction, and the temperature in the valley region is obviously higher than that in the lobe region. Additionally, the water temperature in the back of the lobe is higher than that in the front of the lobe.

1. Introduction

Safety and economy are the key factors affecting the development of nuclear reactor. A good way to enhance the safety and economy of a reactor is to improve the thermal-hydraulic performance of its fuel. In traditional light water reactor (LWR) and boiling water reactor (BWR), the cylindrical fuel is usually adopted. In order to improve the heat transfer characteristic of the fuel assembly, the mixing vane spacer grid is used, which can strengthen the flow mixing between the subchannels in the assembly and raise the critical heat flux of the rod (Qu et al., 2019). However, the resistance to fluid flow in the subchannel also increases because of this. In new generation reactors, some other types of fuels are adopted. For example, in the modular high temperature gas-cooled reactor (MHTGR) and molten salt reactor (MSR), the spherical fuel is adopted (Zhou et al., 2013; Chen et al., 2018), and in sodium-cooled fast reactor (SFR), lead bismuth eutectic (LBE) cooled reactor and supercritical water-cooled reactor (SCWR), the wire-wrapped fuel is adopted (Jeong et al., 2017; Lyu et al., 2016; Podila

and Rao, 2014). Massachusetts Institute of Technology (MIT) proposed an innovative fuel design, internal and external cooled annular fuel, in 2006 (Feng, 2008). The annular fuel can allow a substantial increase in power in pressurized water reactor (PWR) while maintaining or improving safety margins. It has larger surface-to-volume ratio in comparison to the cylindrical fuel. Thus, enlarging the surface-to-volume ratio of the fuel may be an effective approach to increase the power output without necessarily altering the operating surface heat flux (Conboy et al., 2014). The helical cruciform fuel (HCF) also has this feature. It can be used to improve the power density of PWR and BWR.

The cross section of the HCF rod is cruciform shape and it is twisted along the axial direction. This type of fuel was firstly proposed in Russia. Afterwards, it was used in the SM-3 and PIK reactor of Russia (Ageenkov et al., 2002). SM-3 reactor is a high-flux, water-cooled and water-moderated tank-type reactor. Its thermal capacity is 100 MW. It can be used to produce trans-uranium elements and radioactive isotopes of light elements, as well as carry out irradiation studies of reactor material samples (Anatoli, 2014). PIK is also a high-flux research reactor

---

Nomenclature

D_e	equivalent diameter [m]
f	frictional coefficient
G_k	generation of k due to mean velocity gradients
G_ω	generation of ω due to mean velocity gradients
h	heat transfer coefficient [W/(m^2·K)]
k	turbulence kinetic energy [m^2/s^2]
L	length of the channel [m]
q	surface heat flux [W/m^2]
Re	Reynolds number
S_k	user-defined source terms
S_ω	user-defined source terms
T_{bulk}	bulk temperature of water [K]
T_{wall}	wall temperature [K]
v	velocity [m/s]
V_{in}	inlet velocity [m/s]
V_x	velocity in x direction [m/s]
V_y	velocity in y direction [m/s]
Y_k	dissipation of k due to turbulence
Y_ω	dissipation of ω due to turbulence
α	twist angle [°]
β	circumferential angle [°]
Γ_k	effective diffusivity of k [kg/(m·s)]
Γ_ω	effective diffusivity of ω [kg/(m·s)]
ΔP	pressure difference [Pa]
μ	dynamic viscosity [kg/(m·s)]
ρ	density [kg/m^3]
ω	specific dissipation rate [s^{-1}]

Abbreviation

BWR	boiling water reactor
HCF	helical cruciform fuel
LBE	lead bismuth eutectic
LWR	light water reactor
MHTGR	modular high temperature gas-cooled reactor
MSR	molten salt reactor
PWR	pressurized water reactor
SFR	sodium-cooled fast reactor
SCWR	supercritical water-cooled reactor

and its thermal output is 100 MW. It can be used to conduct researches about the weak interaction physics, nuclear physics, condensed matter physics, radiation physics and chemistry, structural and radiation biology and biophysics, and applied engineering. Besides the application in research reactors, the feasibility of the application in Russian icebreaker reactors was also analyzed, so that the high-enriched uranium in reactor fuel could be converted to low-enriched uranium (Diakov et al., 2006). A fast helium cooled reactor concept was developed in Russia, and the application in this reactor was also investigated (Ponomarev-Stepnoi and Glushkov, 2003). Moreover, the pressure drop and heat transfer crisis of a similar fuel rod used in VVER-T reactor was investigated with small-scaled model (Bol' shakov et al., 2007). This fuel rod is three-rayed in the cross section, rather than cruciform shape.

In recent years, MIT also have conducted some researches about the HCF rod. T. M. Conboy et al. (2013) constructed an experimental facility and measured the hydraulic resistance and assembly mixing within a mock HCF bundle. Koroush Shirvan and Mujid S. Kazimi (Shirvan and Kazimi, 2014) benchmarked the data of pressure drop and assembly mixing obtained from this experiment with STARCCM+, and calculated the 3D conduction effect of the HCF rod in steady state and transient condition. In addition, Conboy et al. (2014) also evaluated the power update potential of the HCF core in comparison to the reactor core of

traditional LWR. The results showed that the HCF core could respectively allow power update of 24% for BWR and power update of 47% for PWR within established safety limits. In order to explore the HCF improved performance limits, Koroush Shirvan (2016) investigated the boiling crisis of HCF rods at high pressures with STARCCM+. The results showed that HCF rods could result in maximum power uprate of 25% for PWR and could not result in a benefit for BWR. This result was different from the result in Ref. (Conboy et al., 2014), because the latter is evaluated with 1D empirical correlations.

HCF assembly has a lot of potential advantages (Conboy et al., 2013). Its larger surface can proportionally lower the surface-averaged heat flux at same power. The helical geometry can increase the transverse flow mixing in the bundle, which can homogenize the temperature distribution and reduce the impact of local peaking factors. HCF assembly is a self-supporting assembly, so it needn't spacer grid which is usually used in the cylindrical fuel assembly. Because of this, the pressure drop of the assembly can be reduced. HCF rod has a shorter heat conduction path from the rod center to the coolant, so the maximum temperature of the fuel can also be reduced. Currently, the understanding of the flow and heat transfer characteristics of the HCF assembly is not very thorough, and relevant references are also little. Therefore, it is very essential to further investigate the
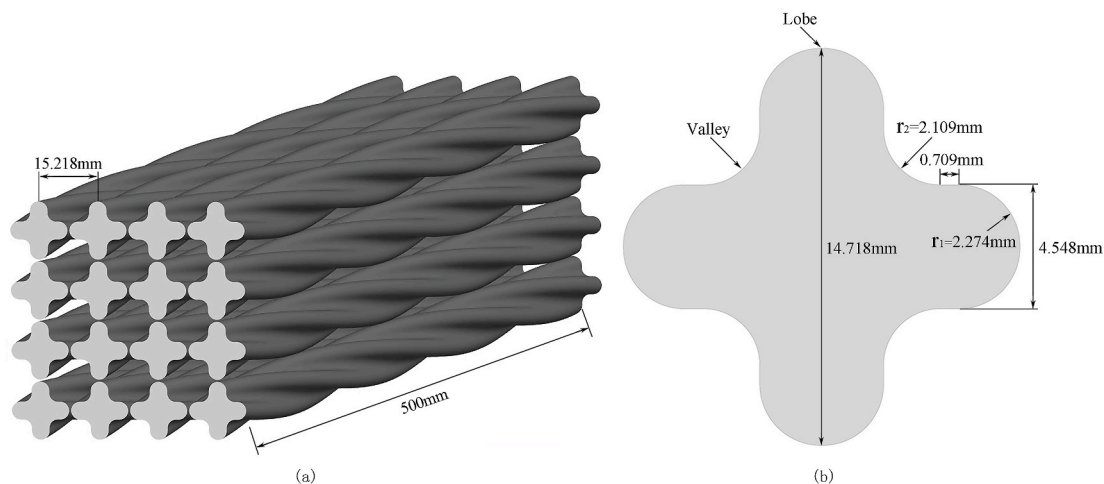

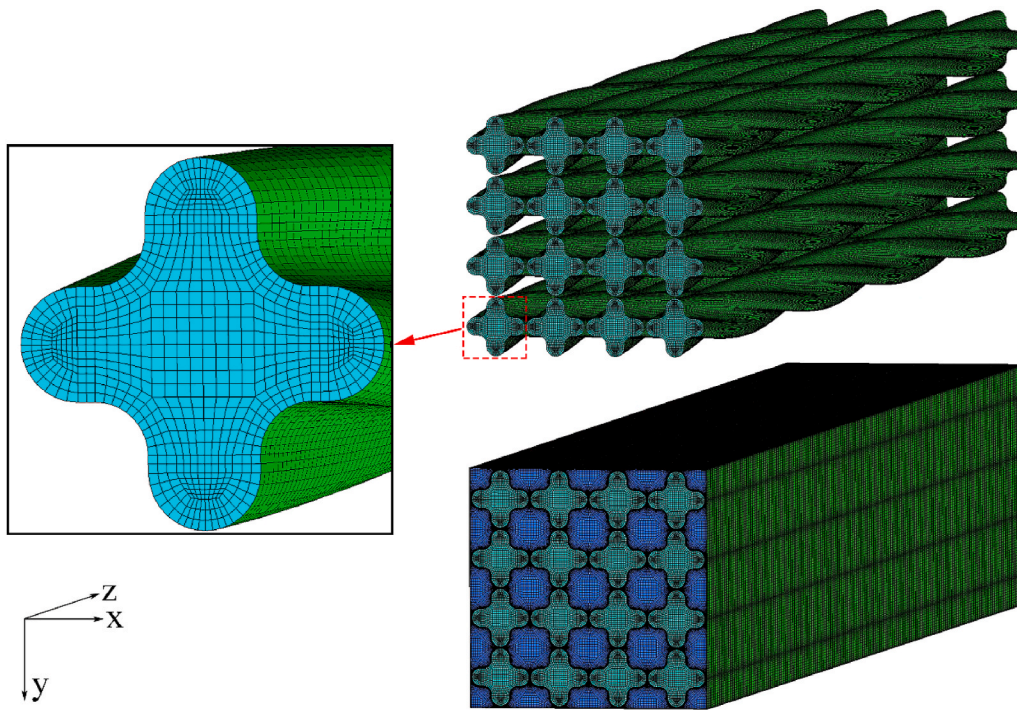**Fig. 1.** (a) HCF bundle; (b) cross section of the HCF rod.

Fig. 2. Grids of the HCF bundle.

thermal-hydraulic performance of the HCF assembly.

This paper is focused on investigating the thermal-hydraulic characteristics of a 4 × 4 HCF bundle by numerical method. Firstly, the numerical model will be developed and validated. Afterwards, transverse flow in the HCF bundle will be analyzed, which is difficult to be exactly shown by experimental method. Meanwhile, the variation of frictional coefficient of the bundle will be given. Finally, temperature distributions of the fuel bundle and the water will be analyzed, and the variation of local heat transfer coefficient will also be given.

2. Methodology

The structure of the HCF bundle in this research is shown in Fig. 1(a), which is obtained from Ref. (Thomas, 2007). As can be seen, this HCF bundle includes 16 HCF rods, and all rods have the same structures. These rods are arranged in rectangular array. The distance between the centerlines of two neighboring rods is 15.218 mm. The cross section of the HCF rod is cruciform, and its detailed parameters are shown in Fig. 1 (b). The maximum diameter of the cross section is 14.718 mm. The convex part and concave part of the rod are respectively named as lobe and valley, which can facilitate the analysis later. With the increase of the rod length, the cross section gradually rotates, resulting in that the rod is finally in helical shape. The twist pitch of the rod is 0.5 m. Considering the periodicity of the rod and the computational cost, the rod length of 0.5 m (one twist pitch) is adopted in this research. This 4 × 4 HCF bundle is placed in a square channel with side width of 61.5 mm. The material of the rod is UO_2, and the coolant is water. Material properties are calculated by using the user-defined function (UDF) of FLUENT, which is a C language function and can be dynamically loaded with the FLUENT solver.

Grids of the HCF bundle are shown in Fig. 2, which are generated by ANSYS ICEM. All the grids are hexahedral volume grids or quadrate surface grids. As can be seen, grids close to the surface of the rods are refined, due to that temperature gradient and velocity gradient of water in this region are greater than those in the other regions. Similarly, grids near the wall of the channel are also refined. In real HCF bundle, there are many contact points between neighboring rods. In order to improve

the quality of the grids, a small gap of 0.5 mm is retained at every contact point in this research. This method has also been adopted by Ref (Gajapathy et al., 2015). and Ref. (Zhao et al., 2017), and the effect of this small gap on the computational result can be neglected. For all grids in the model, the mean grid quality is greater than 0.84, and the minimum is greater than 0.63. Based on the computational result of grid independence, the numerical model contains 28.81 million grids finally.

In the numerical model, the inlet boundary condition is set as the velocity inlet boundary. The outlet boundary condition is set as the pressure outlet boundary, and the value is 0 Pa. Moreover, the four side walls of the channel and the two end surfaces of the HCF bundle are considered as adiabatic wall. Based on the local temperature and pressure, the physical properties of water are calculated. Governing equations of the numerical model are discretized by the finite volume method, and the second order upwind scheme is used for the spatial discretization. For the couple of pressure and temperature, the SIMPLE algorithm is adopted. In the end, the calculation is implemented with ANSYS FLUENT.

In order to investigate the effect of turbulent model on the computational result, the pressure drop experiment in Ref (Thomas, 2007). is simulated by the Realizable k-ε model, Transition SST model and Standard k-ω model in this research, respectively. In this experiment, the operation pressure and temperature of water are respectively 0.1 MPa and 22 °C. According to the range of the Reynolds number in the experiment, five inlet velocities are respectively calculated, which are 1.16 m/s, 1.94 m/s, 2.72 m/s, 3.50 m/s and 4.60 m/s. The Reynolds number, frictional coefficient and local heat transfer coefficient of the HCF bundle are respectively calculated by following equations:

$$Re = \frac{\rho v D_e}{\mu} \tag{1}$$

$$f = \frac{2D_e}{\rho L}\left(\frac{\Delta P}{v^2}\right) \tag{2}$$
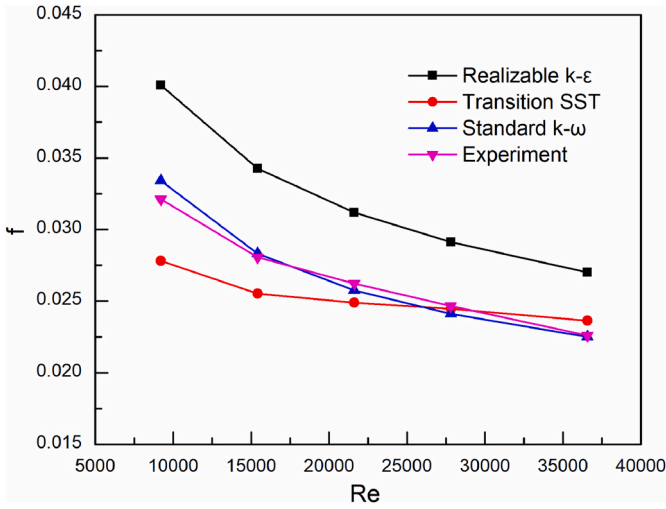
$$h = \frac{q}{(T_{wall} - T_{bulk})} \tag{3}$$

Fig. 3. Frictional coefficient of the HCF bundle.

employed as the wall function.

Governing equations of the fluid flow in the channel adopted in ANSYS FLUENT are shown as follows (ANSYS and Inc, 2011):

Continuity equation:

$$\frac{\partial \rho}{\partial t} + \frac{\partial}{\partial x_i}(\rho u_i) = 0 \tag{4}$$

Momentum equation:

$$\frac{\partial}{\partial t}(\rho u_i) + \frac{\partial}{\partial x_j}(\rho u_i u_j) = -\frac{\partial p}{\partial x_i} + \frac{\partial}{\partial x_j}\left[\mu\left(\frac{\partial u_i}{\partial x_j} + \frac{\partial u_j}{\partial x_i} - \frac{2}{3}\delta_{ij}\frac{\partial u_l}{\partial x_l}\right)\right] + \frac{\partial}{\partial x_j}\left(-\rho\overline{u_i'u_j'}\right) \tag{5}$$

Energy equation:

$$\frac{\partial}{\partial t}(\rho E) + \nabla \cdot (\vec{v}(\rho E + p)) = \nabla \cdot \left(k_{eff}\nabla T - \sum_j h_j \vec{J}_j + (\overline{\tau}_{eff} \cdot \vec{v})\right) + S_h \tag{6}$$

where μ is the dynamic viscosity; k_{eff} is the effective conductivity; $\vec{J}_j$ is the diffusion flux of species j; S_h is the volumetric heat source.

Transport equations for the turbulence kinetic energy (k) and specific dissipation rate (ω) in Standard k-ω model are given by the following expressions:

Turbulent kinetic energy (k):

$$\frac{\partial}{\partial t}(\rho k) + \frac{\partial}{\partial x_i}(\rho k u_i) = \frac{\partial}{\partial x_j}\left(\Gamma_k \frac{\partial k}{\partial x_j}\right) + G_k - Y_k + S_k \tag{7}$$

Specific dissipation rate (ω):

$$\frac{\partial}{\partial t}(\rho \omega) + \frac{\partial}{\partial x_i}(\rho \omega u_i) = \frac{\partial}{\partial x_j}\left(\Gamma_\omega \frac{\partial \omega}{\partial x_j}\right) + G_\omega - Y_\omega + S_\omega \tag{8}$$

where Γ_k and Γ_ω are respectively the effective diffusivity of k and ω; G_k is the generation of k due to mean velocity gradients; G_ω is the generation of ω; Y_k is the dissipation of k due to turbulence; Y_ω is the dissipation of ω; S_k and S_ω are user-defined source terms.

The effective diffusivities for k and ω are given by

$$\Gamma_k = \mu + \frac{\mu_t}{\sigma_k} \tag{9}$$

$$\Gamma_\omega = \mu + \frac{\mu_t}{\sigma_\omega} \tag{10}$$

where ρ is the density; v is the velocity; D_e is the equivalent diameter; μ is the dynamic viscosity; L is the length of the channel; ΔP is the pressure difference between the inlet and outlet; q, T_{wall} and T_{bulk} are respectively the area-averaged surface heat flux, area-averaged wall temperature and mass-averaged cross-sectional temperature of water at one axial location.

The computational result of the frictional coefficient of the HCF bundle is shown in Fig. 3. As can be seen, with the increase of the Reynolds number, the frictional coefficient gradually decreases and all the variation tendencies of the computational results of these three turbulent models are similar with that of the experimental result. However, there are still some errors between the computational result and the experimental result. For the Realizable k-ε model, Transition SST model and Standard k-ω model, the maximum relative errors all occur at the point where Reynolds number is equal to 9222, and the values are 24.83%, 13.40% and 4%, respectively. In the whole range of the Reynolds number, the mean relative errors are 20.72%, 6.56% and 1.87%, respectively. Therefore, the computational result of Standard k-ω model agrees well with the experimental result. In later calculation, only the Standard k-ω model will be adopted, and enhanced wall treatment is
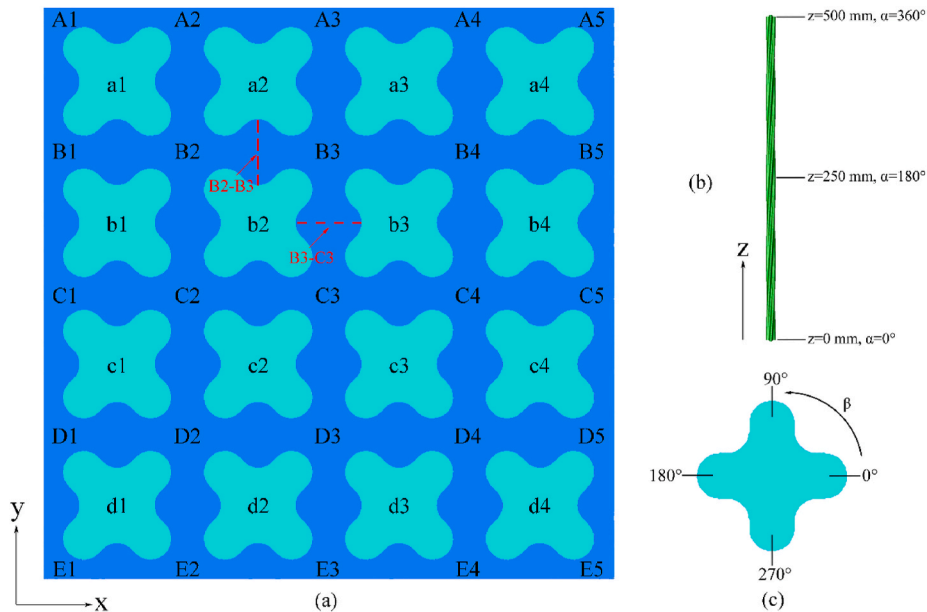

Fig. 4. Nomenclature: (a) HCF rod, subchannel and interface; (b) twist angle; (c) circumferential angle.
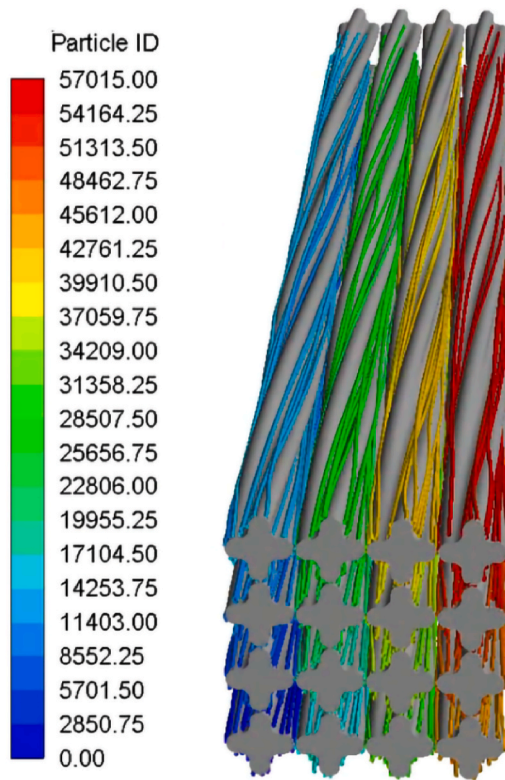
Fig. 5. Pathlines of the water.

where μ_t is the turbulent viscosity; σ_k and σ_ω are respectively the turbulent Prandtl number of k and ω.

3. Results and discussion

Based on the numerical model above, the thermal-hydraulics of the HCF bundle are calculated and analyzed in this research. Five inlet velocities, including 1 m/s, 2 m/s, 3 m/s, 4 m/s and 5 m/s, are respectively calculated. The operation pressure and inlet temperature of water are respectively set as 15.51 MPa and 565.85 K. Moreover, the volume heat flux of the bundle is set as 2.0×10^8 W/m³.

In order to make it convenient to analyze the computational results, the rods and subchannels in the HCF bundle are named as shown in Fig. 4(a). The name of subchannel is composed of capital letter and number, and the name of rod is composed of lower-case letter and number. The interface between two subchannels is named by the names of these two subchannels. For example, the interface between subchannel B3 and C3 is named as B3–C3. Along the length of the fuel rod, the position of the lobe moves (rotates) counter clockwise when it is viewed from the top. This angle is defined as twist angle (α), as shown in Fig. 4(b). With the increase of the axial (+z) position, the twist angle also gradually increases. There is a one-to-one correspondence between twist angle and axial position. Therefore, the twist angle gradually varies along the length of the rod. When the axial positions are 0 mm, 250 mm and 500 mm, the twist angles are 0°, 180° and 360°, respectively. Fig. 4 (c) shows the definition of circumferential angle (β), which can be used to indicate the position of one point on the surface of the rod at one cross-section. The 0° is corresponding to the +x direction.

3.1. Flow analysis

Fig. 5 shows the pathlines of the water when the inlet velocity is equal to 5 m/s. It can be seen that the water rotates along the surface of the HCF rod when it flows forward. This phenomenon can enhance the transverse mixing of the water in the bundle, which will be helpful for reducing the temperature difference between different subchannels.

The transverse velocity vectors at different twist angles are shown in Fig. 6. As can be seen, a strong transverse flow occurs in the valley region of the rod, because this region is adjacent to the side of the lobe. The transverse flow rotates around the rod and its direction is identical with the twist direction. At the gap between two neighboring rods, two regions with opposite flow direction simultaneously occurs. The reason for this phenomenon is that the twist directions of two neighboring rods are just opposite at the gap. Due to that the center region of the subchannel is far from the rod lobe, the effect of the lobe on the flow is small, so the transverse flow in this region is not very obvious. In the range between 180° and 225°, with the increase of the twist angle, the gap between two neighboring rods gradually increases, resulting in that the flow mixing between two neighboring subchannels are gradually strengthened. In this process, the variation of the transverse velocity in the valley region of the rod is very small. As shown in Fig. 6, when twist angle is equal to 180°, the gap has the smallest width, while it has the largest width when twist angle is equal to 225°. In the range of the whole length of the bundle, the gap between two neighboring rods periodically varies with the increase of the twist angle, as shown in Fig. 7. It is an increase process of the gap when twist angle increases from 180° to 225°, while when twist angle increases from 225° to 270°, it is a decrease process. Thus, every 90° is a variation cycle. Under the effect of the periodic variation of the gap, the intensity of the flow mixing between two neighboring subchannels also periodically varies.

Fig. 8 shows the velocity distributions in interface B3–C3 between twist angle of 180° and 270° (z = 250 mm ~ z = 375 mm), in which Fig. 8(a) and (b) are respectively the velocity distributions of x direction and y direction. In Fig. 8(a), the flow directions on the left and right side are opposite at same twist angle, which is same as shown in Fig. 6. With the increase of the twist angle, the flow direction on one side periodically varies. On the left side, it is along the +x direction at the beginning. Afterwards, it gradually changes to the -x direction. Then, it gradually changes to the +x direction and -x direction again. The variation tendency on the right side is just opposite. Thus, there are two variation cycles for the velocity of x direction. The whole variation process can be divided into four parts. In every part, there is a pair of regions in which the flow directions are opposite. The velocity distribution of y direction is different from that of x direction, as shown in Fig. 8(b). The flow direction on the left side is along the -y direction throughout all twist angles, and the direction on the right side is along the +y direction. There is only one pair of regions with opposite flow directions. With the increase of the twist angle, the value of the velocity increases firstly, and then, it gradually decreases. This process forms the only variation cycle.

The variation of the transverse velocity in interface B3–C3 is shown in Fig. 9, in which the velocity at every twist angle is the mean velocity at this twist angle (the surface average value over constrained plane). It can be seen that the transverse flow has obvious periodicity under the conditions of different inlet velocities, and the larger the inlet velocity is, the stronger the transverse flow is. There are four cycles in the twist angles of 360°. In every cycle, the variations of twist angle for the increase process and decrease process of the velocity in -y direction are nearly same. The value of the velocity is less than 0 throughout, which means that the net flow in y direction in this interface is always along the -y direction. The peak value and valley value of the velocity in x direction respectively occurs in the front and back of the peak value in -y direction. Differing from that in -y direction, the peak value in x direction is greater than 0, while the valley value is less than 0. It indicates that the net flow in x direction is alternately along the +x direction and the -x direction. Moreover, it also can be seen that the transverse flow in -y direction is stronger than that in +x direction in this interface. The peak value of the velocity in -y direction is more than twice of that in +x direction. In Fig. 9, the transverse velocity at 0° is equal to 0, which is due to that the velocity inlet boundary is adopted as the inlet boundary condition of the numerical model. In future research, the periodical
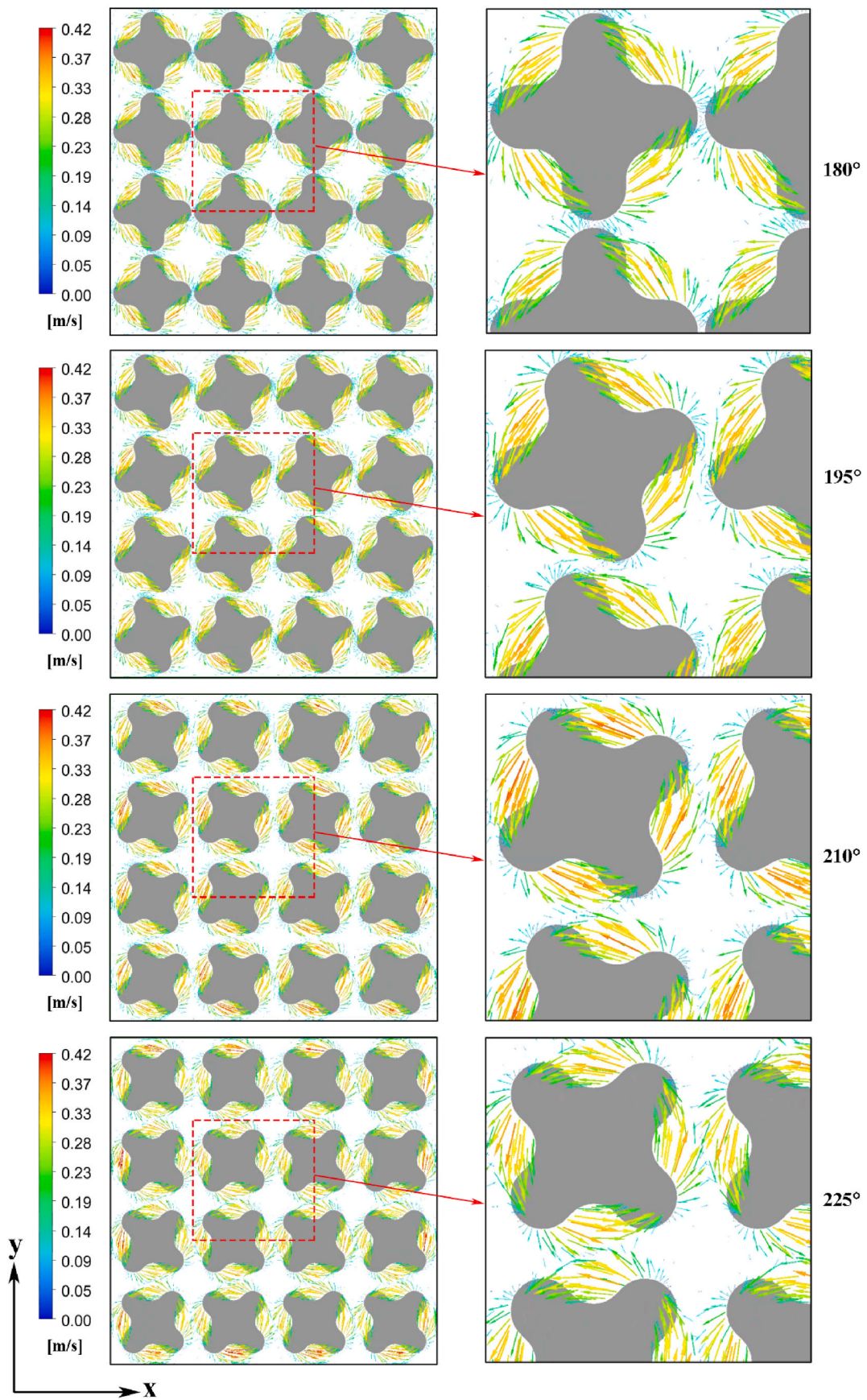
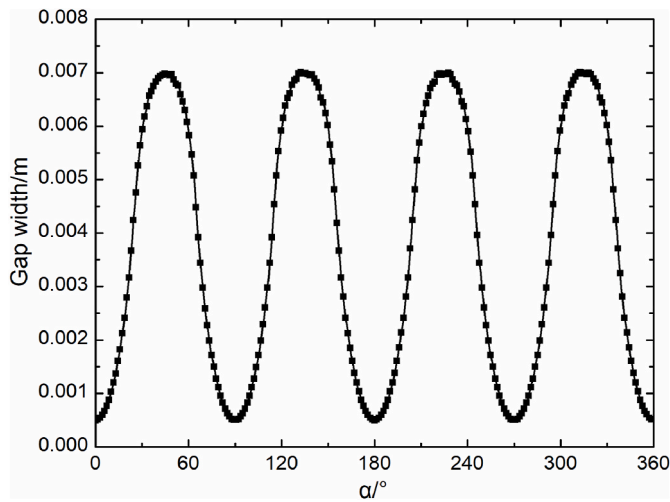**Fig. 6.** Transverse velocity vectors at different twist angles.
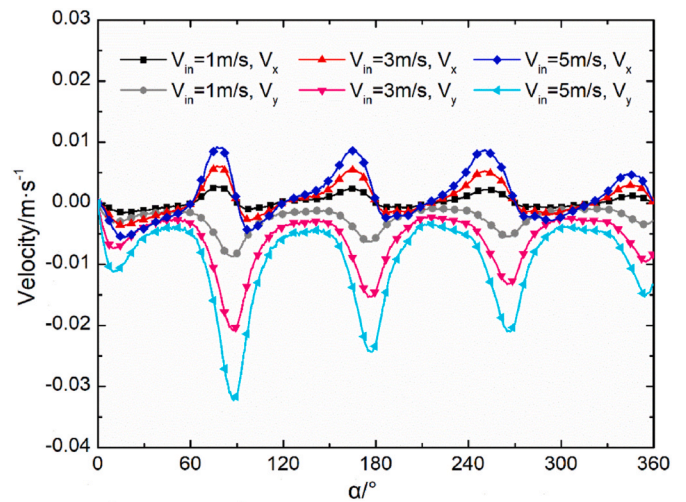
Fig. 7. Variation of gap width.

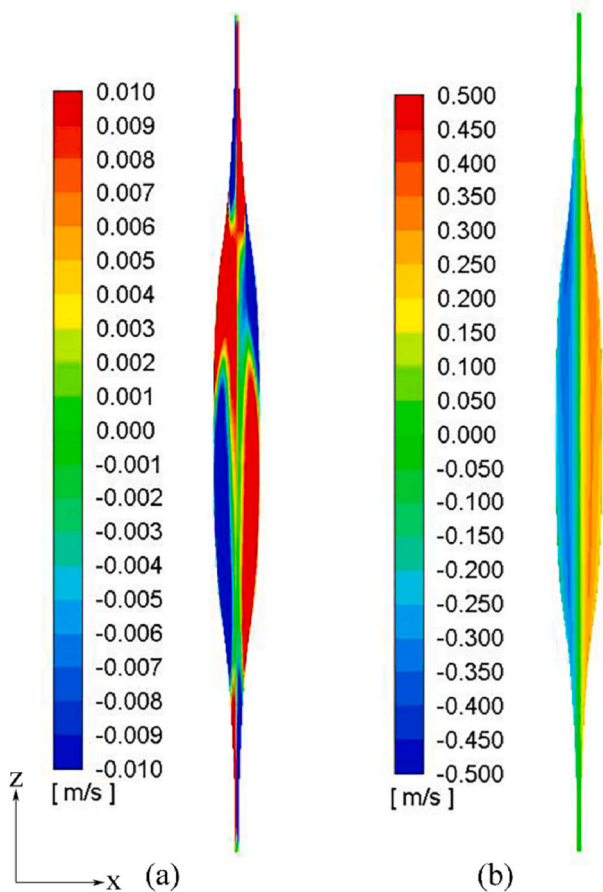Fig. 9. Variation of the transverse velocity in interface B3–C3.

Fig. 8. Velocity distributions in interface B3–C3: (a) x direction; (b) y direction.

Fig. 10. Variation of the transverse velocity in interface B2–B3.

Fig. 11. Frictional coefficient of the HCF bundle.

boundary will be adopted, so that the entrance effect can also be eliminated.

Fig. 10 shows the variation of the transverse velocity in interface B2–B3. The transverse velocity in this interface also varies periodically. Different from the phenomenon in interface B3–C3, the value of the velocity in x direction in this interface is greater than 0 throughout, while the value of the velocity in y direction alternately varies between negative number and positive number. It indicates that the net flow in x direction in this interface is always along the +x direction, while the net
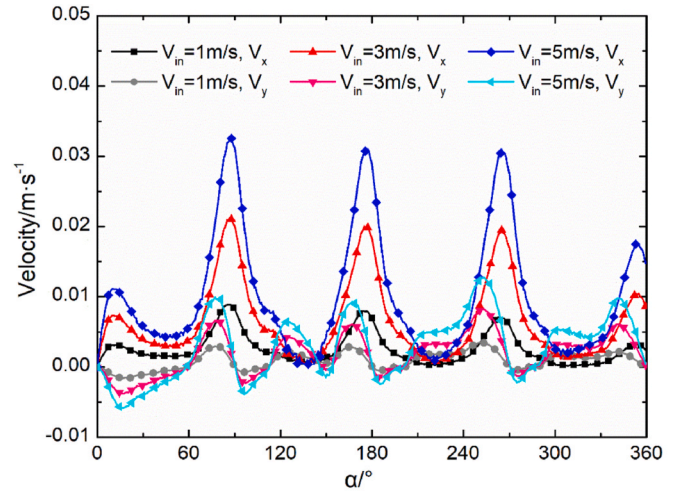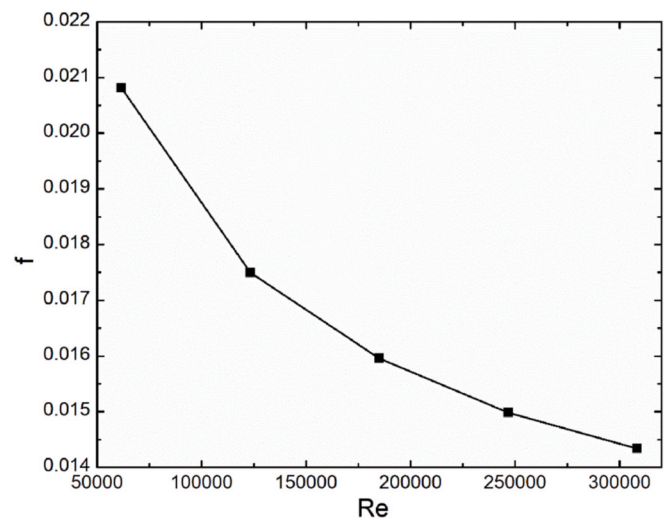
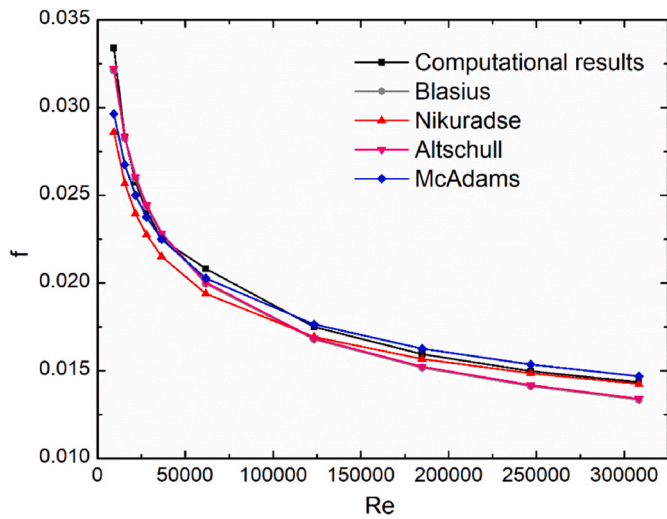flow in y direction is alternately along the -y direction and the +y

Fig. 12. Frictional coefficient of the HCF bundle.

direction. Meanwhile, the twist angle occupied by the flow in +y direction is greater than that occupied by the flow in -y direction, and peak value of the velocity in +y direction is also greater than that in -y direction, which indicates that in most locations, the flow in y direction is along the +y direction. The transverse flow in +x direction is stronger than that in +y direction. The peak value of the velocity in +x direction is more than three times of that in +y direction. With the inlet velocity increasing, the difference between the velocities in +x direction and in +y direction also gradually rises.

Fig. 11 shows the variation of the frictional coefficient of the HCF bundle. As can be seen, the frictional coefficient gradually decreases with the increase of the Reynolds number, and the decrease rate also gradually diminishes. When Reynolds number increases from 61,675 to

308,376, the frictional coefficient decreases from 0.0208 to 0.0143. The result in this figure can merge with the result in Fig. 3, forming a new variation curve which can be used in a wider range of Reynolds number, as shown in Fig. 12. The variation range of Reynolds number in this new curve is 9222–308,376. The computational results are validated with four empirical correlations, which are Blasius correlation, Nikuradse correlation, Altschull correlation and McAdams correlation, respectively. These correlations can be found in Ref (Thomas, 2007). and Ref. (Kong, 2007). It can be seen that the computational results agree well with the results of Blasius correlation and Altschull correlation when Reynolds number is less than 40,000. The relative errors between them are within 3.9%. When Reynolds number is more than 22,000, the computational results agree well with the results of McAdams correlation, and the relative errors are within 2.9%. For the results of Nikuradse correlation, the relative errors are within 3.3% when Reynolds number is more than 130,000. Therefore, by choosing the most appropriate one based on Reynolds number, these correlations can be used to calculate the frictional coefficient of the HCF bundle.

3.2. Heat transfer analysis

Temperature distribution on the surface of the HCF bundle is shown in Fig. 13, in which the inlet velocity is 5 m/s. As can be seen, the temperature distribution also helically varies along the flow direction. On the surface in the valley region, the temperature is higher than that in the lobe region. Along the flow direction, the increase rate of the temperature in the valley region is also higher. The reason for this phenomenon is that the surface area in the valley region is relative smaller, which is detrimental to the dissipation of heat. This phenomenon is more obvious inside the bundle. At twist angle of 135° and 360°, the temperature at the top of the lobe is distinctly lower than those in other regions. Fig. 14 shows the temperature variations on the surface of rod b2 at twist angle of 135° and 360°. It can be seen that the temperature periodically varies along the circumferential direction. The peak value
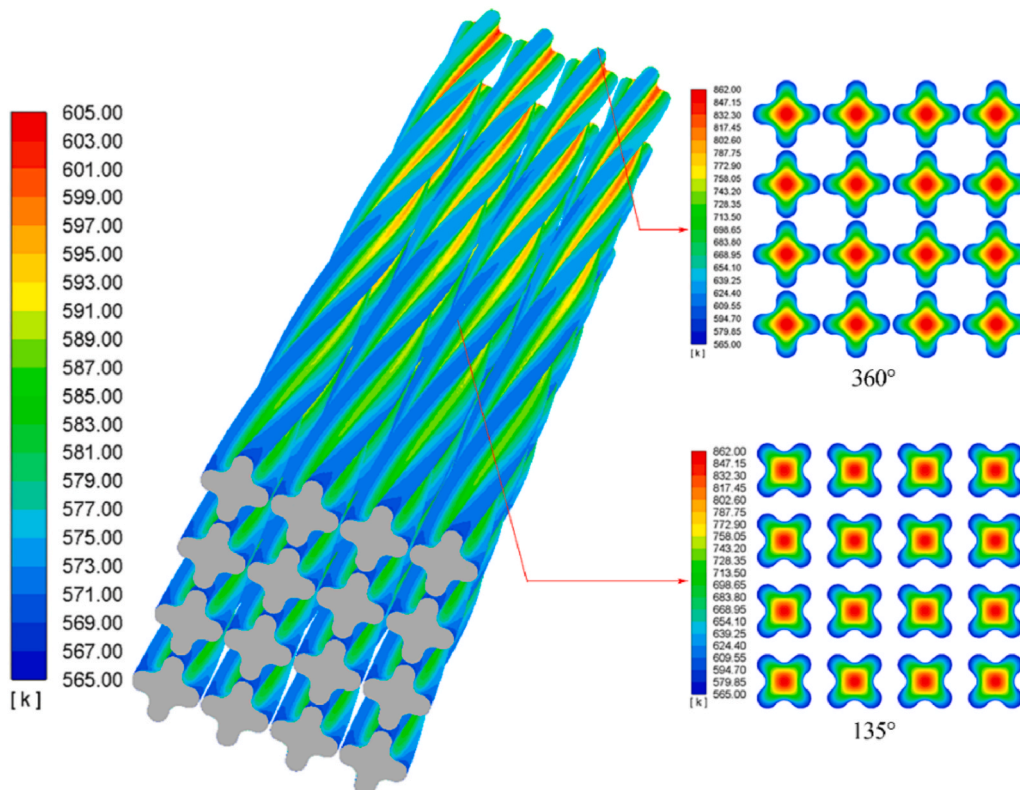

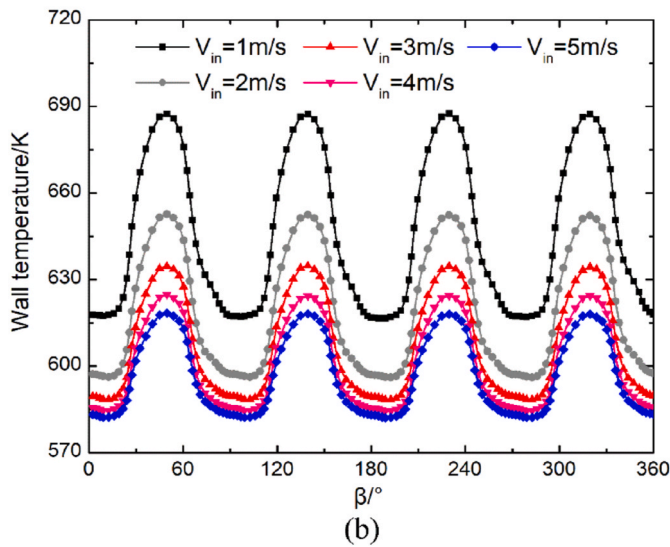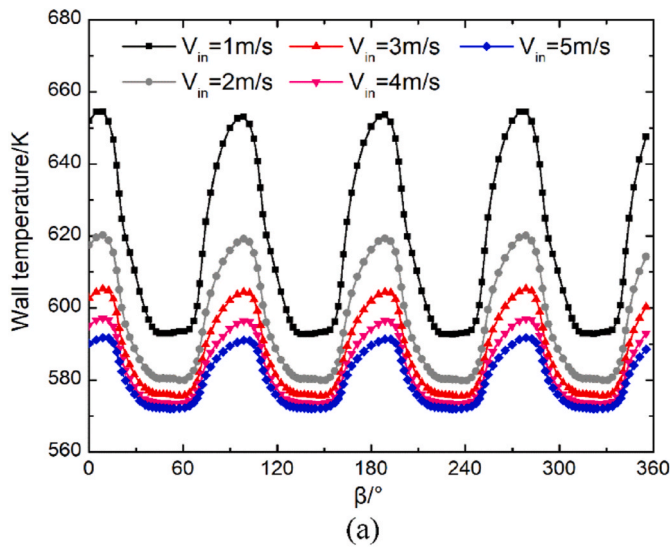**Fig. 13.** Temperature distribution on the surface of the HCF bundle.

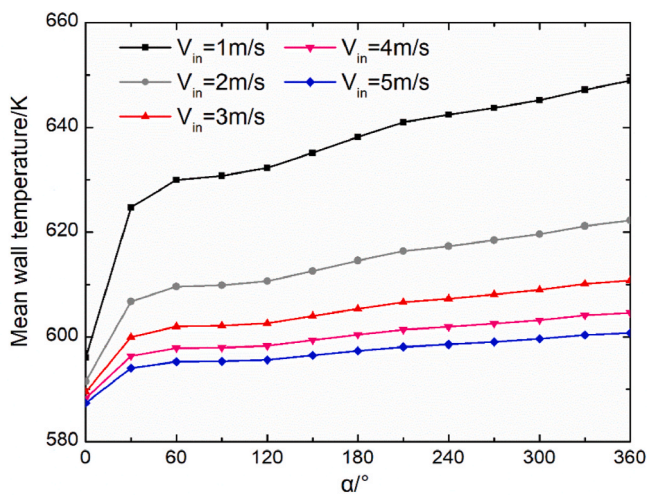**Fig. 14.** Temperature variations on the surface of rod b2 at different twist angles: (a) 135°; (b) 360°.

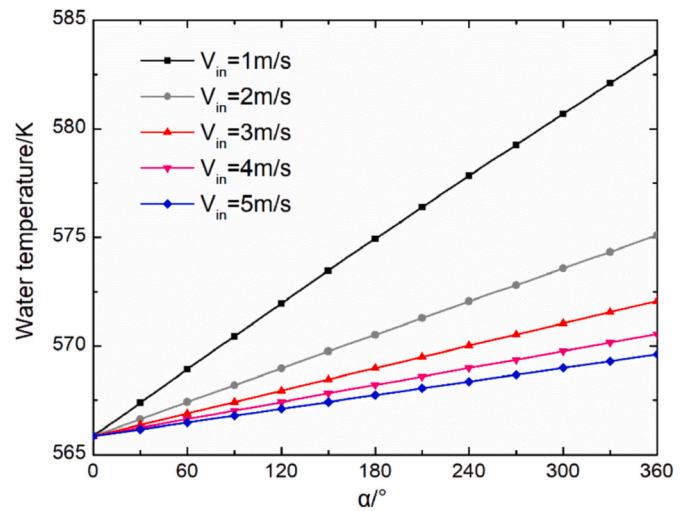**Fig. 15.** Variation of the mean wall temperature of the HCF bundle.

Fig. 16. Variation of water temperature.

in the curve is the temperature near the bottom of the rod valley, and the valley value is the temperature near the top of the rod lobe. Thus, there are four variation cycles in one circumference. At both twist angles, the wall temperature decreases with the increase of inlet velocity, and the decreasing extent also diminishes. Moreover, the difference between the peak value and the valley value also gradually decreases, which means that the flow mixing in the HCF bundle is strengthened. At twist angle of 135°, this difference decreases from 61.0 K to 19.5 K when inlet velocity increases from 1 m/s to 5 m/s. At twist angle of 360°, this difference decreases from 70.4 K to 36.0 K. For the same inlet velocity, this difference gradually increases with the increase of twist angle.

The variation of the mean wall temperature of the HCF bundle is shown in Fig. 15, in which the mean wall temperature is calculated by the area-weighted average method. In the region near the inlet, the boundary layer has not been fully developed, so it is relatively thin compared to those in other regions, which is good for the heat transfer between the wall and the fluid. As can be seen, due to the influence of entrance effect, heat transfer process near the inlet is enhanced, so the wall temperature in this region is obviously lower than those in other regions. When twist angle is more than 30°, the mean wall temperature approximatively linearly rises with twist angle increasing, and the rising rate gradually decreases with the increase of inlet velocity. It is caused by the variation of water temperature, as shown in Fig. 16, in which the temperature at one twist angle is the average value at this twist angle. It can be seen that the water temperature linearly increases with the increase of twist angle. When inlet velocity rises, both the water temperature and its increasing rate decrease, because the heat power of the rod is constant.

Fig. 17 shows the temperature distributions of water at different twist angles when inlet velocity is equal to 5 m/s. In this figure, the twist direction is along the anticlockwise direction. As can be seen, the temperature in the valley region of the rod is higher than that in the center region of the subchannel, because the valley region is adjacent to the rod. With the increase of twist angle, the temperature in the back of the lobe is higher than that in the front of the lobe. The reason is that the water in the back of a lobe partly comes from the front of the latter lobe, and this part of water has absorbed some heat from the latter lobe. The variation of the local heat transfer coefficient of the HCF bundle is shown in Fig. 18. As can be seen, the local heat transfer coefficient near the inlet is relatively high due to the entrance effect. It gradually decreases with the twist angle increasing. When twist angle is more than 60°, the local heat transfer coefficient increases firstly, and then gradually decreases again with the twist angle further increasing. With inlet velocity rising, the local heat transfer coefficient gradually increases, but the increasing rate gradually decreases. Therefore, the entrance effect
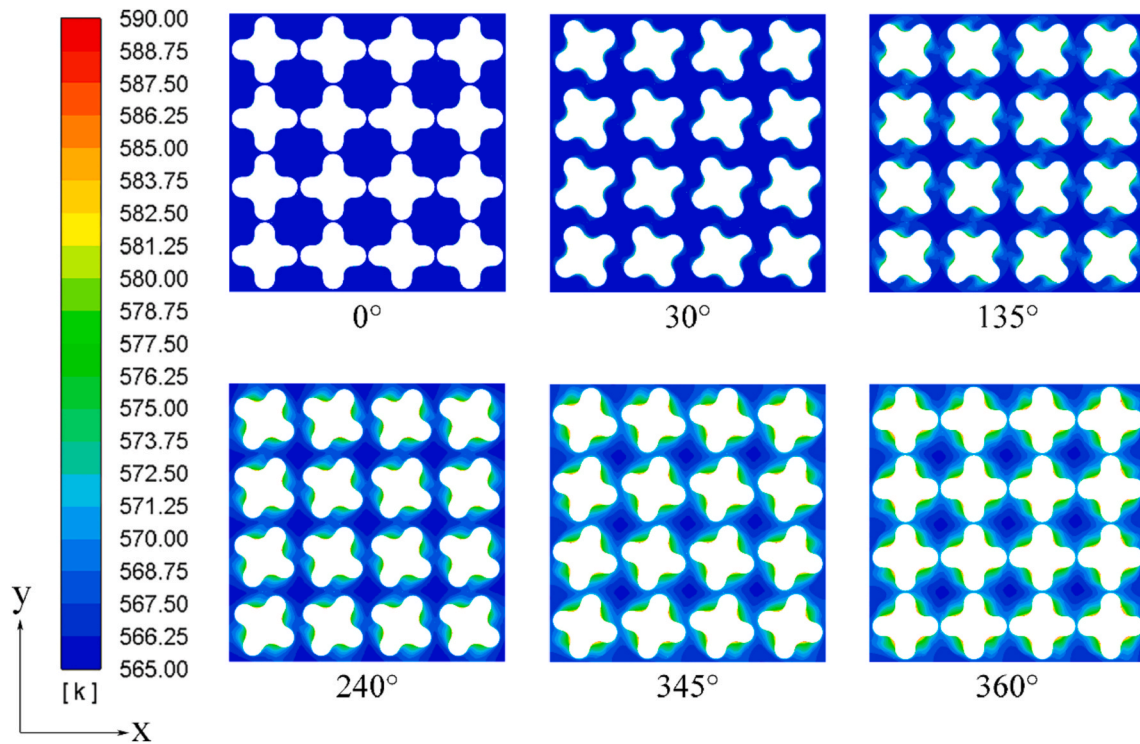
Fig. 17. Temperature distributions of water at different twist angles.
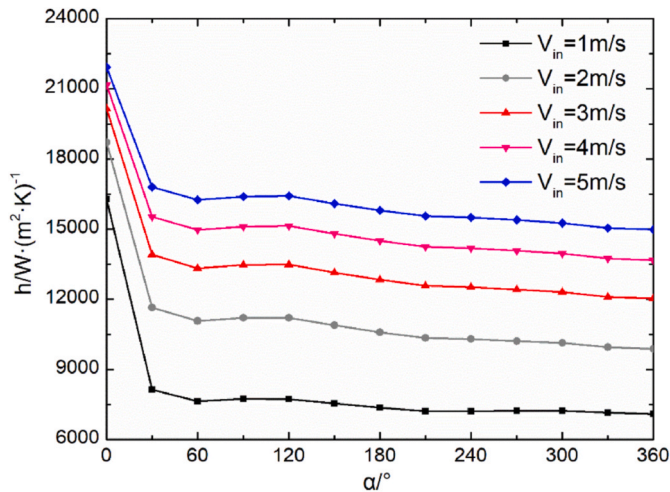

Fig. 18. Variation of local heat transfer coefficient of the HCF bundle.

has a great influence on the local heat transfer coefficients of the HCF bundle.

4. Conclusion

The thermal-hydraulic characteristics of a 4 × 4 HCF bundle were investigated by numerical method in this research. A numerical model of the bundle was developed, and it was validated with the experimental data in Ref. (Thomas, 2007). Based on this model, five flow conditions were respectively calculated. According to the computational results, the transverse flow in the HCF bundle was analyzed, and the temperature distributions of the fuel bundle and the water were discussed. Moreover, the variations of the frictional coefficient and the local heat transfer coefficient of the bundle were also given. The main conclusions from this research are listed as follows:

(1) Due to the helical geometry of the HCF rod, the water rotates along the rod surface when it flows forward. The transverse mixing of water in the bundle is enhanced because of this. In the valley region of the rod, the transverse flow is strong, while it is not very obvious in the center region of the subchannel, because the transverse flow is mainly caused by the rod lobe.

(2) Under the effect of the periodic variation of the gap, the intensity of the flow mixing between two neighboring subchannels also periodically varies, and every twist angle of 90° is a variation cycle.

(3) In every variation cycle of the gap in interface B3–C3, there are four pairs of regions in which the flow directions are opposite in x direction, while there is only one pair of regions with opposite flow directions in y direction. Moreover, with the increase of the twist angle, the net flow in x direction is alternately along the +x direction and the -x direction in this interface, while the net flow in y direction is always along the -y direction. In interface B2–B3, the net flow in x direction is always along the +x direction, while the net flow in y direction is alternately along the -y direction and the +y direction.

(4) The temperature distribution on the rod surface also helically varies along the flow direction, and the temperature in the valley region is obviously higher than that in the lobe region. At one twist angle, temperature periodically varies along the circumferential direction. There are four variation cycles in one circumference. Additionally, the water temperature in the back of the lobe is gradually higher than that in the front of the lobe with twist angle increasing.

Declaration of competing interest

The authors declare that they have no known competing financial interests or personal relationships that could have appeared to influence the work reported in this paper.

Acknowledgements

References

Ageenkov, V.I., Volkov, V.S., Solonin, M.I., Garusov, E.A., Zvezdkin, V.S., Konoplev, K.A., Bek, E.G., Il'yashik, M.I., Potoskaev, G.G., Samokhin, M.G., Tsibulya, V.A., 2002. Parameters and technology for fabricating PIK reactor fuel elements. Atom. Energy 92, 468–474.

Anatoli, S., 2014. Diakov, prospects for conversion of HEU-fueled research reactors in Russia. Sci. Global Secur. 22, 166–187.

ANSYS, Inc, 2011. ANSYS FLUENT Theory Guide 14.0.

Bol'shakov, V.V., Bashkirtsev, S.M., Kobzar', L.L., Morozov, A.G., 2007. Experimental study of burnout in channels with twisted fuel rods. Therm. Eng. 54, 386–389.

Chen, Xingwei, Zou, Yang, Yan, Rui, Liu, Fengrui, Zhang, Jie, Mei, Mudan, Cai, Xiangzhou, 2018. The packing factor of the pebble bed in molten salt reactor. Ann. Nucl. Energy 122, 118–124.

Conboy, T.M., McKrell, T.J., Kazimi, M.S., 2013. Experimental investigation of hydraulics and lateral mixing for helical-cruciform fuel rod assemblies. Nucl. Technol. 182, 259–273.

Conboy, T.M., McKrell, T.J., Kazimi, M.S., 2014. Evaluation of helical cruciform fuel rod assemblies for high-power-density LWRs. Nucl. Technol. 188, 139–153.

Diakov, Anatoli C., Dmitriev, Alexander M., Kang, Jungmin, Shuvayev, Alexey M., von Hippel, Frank N., 2006. Feasibility of converting Russian icebreaker reactors from HEU to LEU Fuel. Sci. Global Secur. 14, 33–48.

Feng, Bo, 2008. On the Use of High Performance Annular Fuel in PWRs. Massachusetts Institute of Technology, Cambridge.

Gajapathy, R., Velusamy, K., Selvaraj, P., Chellapandi, P., 2015. CFD investigation of effect of helical wire-wrap parameters on the thermal hydraulic performance of 217 fuel pin bundle. Ann. Nucl. Energy 77, 498–513.

Jeong, Jae-Ho, Song, Min-Seop, Lee, Kwi-Lim, 2017. CFD investigation of three-dimensional flow phenomena in a JAEA 127-pin wire-wrapped fuel assembly. Nucl. Eng. Des. 323, 166–184.

Kong, Long, 2007. Engineering Fluid Mechanics, third ed. China Electric Power Press, Beijing.

Lyu, Kefeng, Chen, Liuli, Yue, Chenchong, Gao, Sheng, Zhou, Tao, Huang, Qunying, 2016. Preliminary thermal-hydraulic sub-channel analysis of 61 wire-wrapped bundle cooled by lead bismuth eutectic. Ann. Nucl. Energy 92, 243–250.

Podila, K., Rao, Y.F., 2014. Assessment of CFD for the Canadian SCWR bundle with wire wraps. Prog. Nucl. Energy 77, 373–380.

Ponomarev-Stepnoi, Nikolai N., Glushkov, Evgeny S., 2003. Development of fast helium cooled reactors in Russia. In: International Conference on Nuclear Energy for New Europe, Portorož, Slovenia, September 8-11.

Qu, Wenhai, Wang, Zefeng, Xiong, Jinbiao, Cheng, Xu, 2019. Experimental study of cross flow and lateral pressure drop in a 5×5 rod bundle with mixing vanes pacer grid. Nucl. Eng. Des. 353, 110209.

Shirvan, Koroush, 2016. Numerical investigation of the boiling crisis for helical cruciform-shaped rods at high pressures. Int. J. Multiphas. Flow 83, 51–61.

Shirvan, Koroush, Kazimi, Mujid S., 2014. Three dimensional considerations in thermal-hydraulics of helical cruciform fuel rods for LWR power uprates. Nucl. Eng. Des. 270, 259–272.

Thomas, M., 2007. Conboy, Thermal-Hydraulic Analysis of Cross-Shaped Spiral Fuel in High Power Density BWRs. Massachusetts Institute of Technology, Cambridge.

Zhao, Pinghui, Liu, Jiaming, Ge, Zhihao, Wang, Xi, Cheng, Xu, 2017. CFD analysis of transverse flow in a wire-wrapped hexagonal seven-pin bundle. Nucl. Eng. Des. 317, 146–157.

Zhou, Xiangwen, Lu, Zhenming, Zhang, Jie, Liu, Bing, Tang, Chunhe, Zou, Yanwen, Tang, Yaping, 2013. Preparation of spherical fuel elements for. HTR-PM in INET 263, 456–461.